Engineering Failure Analysis 123 (2021) 105322

Contents lists available at ScienceDirect

Engineering Failure Analysis

journal homepage: www.elsevier.com/locate/engfailanal

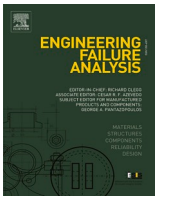

Review

Study on damage tolerance and remain fatigue life of shattered rim of railway wheels

Tao Cong [a], Xiaolong Liu [b,*], Si Wu [a], Guanzhen Zhang [a], Erqing Chen [b], Guian Qian [c,*], Filippo Berto [d]

[a] Metals and Chemistry Research Institute, China Academy of Railway Sciences Corporation Limited, Beijing 100081, China
[b] School of Mechanical, Electronic and Control Engineering, Beijing Jiaotong University, Beijing 100044, China
[c] State Key Laboratory of Nonlinear Mechanics (LNM), Institute of Mechanics, Chinese Academy of Sciences, Beijing 100190, China
[d] Department of Mechanical and Industrial Engineering, Norwegian University of Science and Technology (NTNU), Richard Birkelands vei 2b, 7491 Trondheim, Norway

ARTICLE INFO

Keywords:
Wheel
Shattered rim
Crack propagation
Damage tolerance
Fatigue life evaluation

ABSTRACT

The shattered rim on railway wheels is increasingly concerned in recent years. Based on the failure analysis, the mechanism of shattered rim was revealed. The contact stress distribution of wheel/rail with inclusions in the wheel was analyzed by ABAQUS. Then the stress field was imported into FRANC3D to simulate the crack propagation. It is found that the simulation results were in good agreement with those obtained experimentally from the actual shattered rim, which proves the availability of the simulation. Meanwhile, the influence of the size and location of the inclusions on the fatigue life of the wheel was evaluated. Based on the crack propagation curves obtained by simulation, the rolling contact fatigue damage tolerance analysis and remaining fatigue life assessment method of wheels were proposed.

1. Introduction

According to the location of initiation of fatigue cracks, three fatigue types in wheel have been defined from several fatigue failures of railway wheel, i.e., spalling on the tread [1–5], shelling in the subsurface of rim [6–10], shattered rim in interior of rim [11–19] as shown in Fig. 1. The cracks of shattered rim and shelling are generally caused by inclusions. Normally, the stability of trains is affected by the detachment of material due to spalling and shelling on the tread. However, shattered rim can lead to derailment or other severe train accidents. Therefore, the assessment of propagation life of shattered rim cracks is an important basis for wheel maintenance. Accurately predicting the fatigue life of railway wheels has always been an important but difficult issue for railway.

At the early stage, shattered rims are not easily detected, but once they are found, the consequences are very serious. Thus shattered rims are the key research objects for damage tolerance and remaining fatigue life of a wheel [20,21]. Since the early cracks originated inside the rim, UT inspection can only be used for detection at present, and there is no theoretical basis. As long as a crack with an internal diameter of 3 mm is detected, the wheel is judged to be invalid. The size of the shattered rim crack and the detection cycle are also lack of theoretical basis.

There are two basic methods for analyzing shattered rim damage tolerance and remaining fatigue life. The first one is Murakami analysis method based on the fatigue failure theory [22]. Based on a large number of experimental data, the empirical formula of

* Corresponding authors.
E-mail addresses: liuxiaolong@bjtu.edu.cn (X. Liu), qianguian@imech.ac.cn (G. Qian).

https://doi.org/10.1016/j.engfailanal.2021.105322
Received 14 October 2020; Received in revised form 31 December 2020; Accepted 20 January 2021
Available online 24 February 2021

material fatigue limit σ_w is summarized, and the effect of defects on wheel rim fatigue performance is considered. The influence of defects on wheel damage is generally analyzed by finite element calculation and multi-axis fatigue theory. Murakami formula is an empirical formula obtained through axial fatigue test, while the main driving force of rim crack is shear force [22]. Therefore, there may be some deviation in evaluating the critical size of inclusions in the shattered rim according to the Murakami formula. Another analysis method is based on linear elasticfracture mechanics method. Because the plastic deformation region at the rim crack tip is very small, the theory of linear elastic fracture mechanics is applicable to the study of rim crack. Some researchers [23–25] believe that the rim crack is a kind of mix crack. When the amplitude of equivalent stress intensity factor of the mix crack exceeds the threshold value of the material, the crack begins to initiate.

In this paper, the failure analysis of wheels with shattered rim in actual line was conducted, and the failure mechanism of shattered rim was revealed. Based on fracture mechanics, the research was carried out by finite element simulation which has been widely used in the field of strength design of high speed train [26–28] and has been widely recognized. Firstly, the software ABAQUS was used to help us to get the wheel-rail contact stress, which was then imported into the software FRANC3D to conduct the simulation of shattered rim crack propagation. The simulation results were compared with the actual rim crack failure ones, and they agree well with each other, which verify the validation of the simulation. At the same time, the influence of the initial crack size and location on the fatigue life of the wheel was studied, and the evaluation method of the damage tolerance and remaining life of the wheel rim crack was given.

2. Shattered rim on revenue railway

2.1. Shattered rim case

A shattered rim on the revenue railway in China was successfully detected by the online inspection. The train wheel ran for 450,000 km. Its area was about 30 mm × 40 mm, and the depth was about 17 mm as shown in Fig. 2. The defect area locates in the red rectangle. In order to explore the specific causes and conditions of the failure, the shattered rim failure analysis was carried out. Firstly, the part of the rim with flaw was cut out by the cutting machine. Then, the accurate location of shattered rim was determined via UT inspection, and its crack was opened to observe the fatigue surface. Finally, the inclusion type at the crack initiation zone was analyzed by SEM and EDS. According to the above analysis, the size and location of the defect causing rim crack failure can be gradually determined, which provides a basis for further analysis of the remaining fatigue life of shattered rim wheel.

2.2. Shattered rim mechanism

Depending on the results of UT inspection, the fatigue crack surface was opened by sawing, and its morphology was shown in Fig. 3. It was called non-penetrating shattered rim which The crack is still in the interior of the wheel and can only be detected by ultrasonic devices [23]. Its crack surface can be obviously seen fatigue initiation zone, and the propagation zone was not corroded due to non-contact with atmosphere. It is the typical fatigue feature with internal initiation zone and beach bands. The location of the crack initiation zone was 16.7 mm from the tread and 60.3 mm from the outer side of rim.

The crack surface of shattered rim was observed by the scanning electron microscope (SEM).

Fig. 4 presents that there was a complex inclusion with size of 1.54 mm in length and 0.25 mm in width. The EDS result declared that the inclusion was mainly composed of aluminum oxide.

It presents the schematic for the formation mechanism of shattered rim caused by defects in Fig. 5. When the location of defect is at the depth of less than 10 mm from the tread, the crack will prefer to propagate to the tread since the stress near the tread is larger than that far away from the tread. This damaged tread can continue to work after recondition. When the defect is inside the wheel and its depth exceeds 10 mm, the crack will propagate to the rim, which is called shattered rim. It will lead to wheel failure and even train accidents.

Fig. 1. Three fatigue types in wheel, (a) spalling on the tread, (b) shelling in the subsurface of rim and (c) shattered rim in interior of rim.

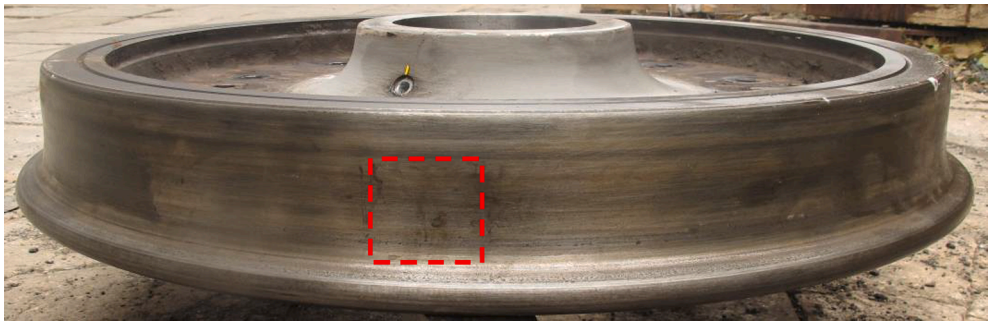

Fig. 2. Shattered rim and morphology of the defect.

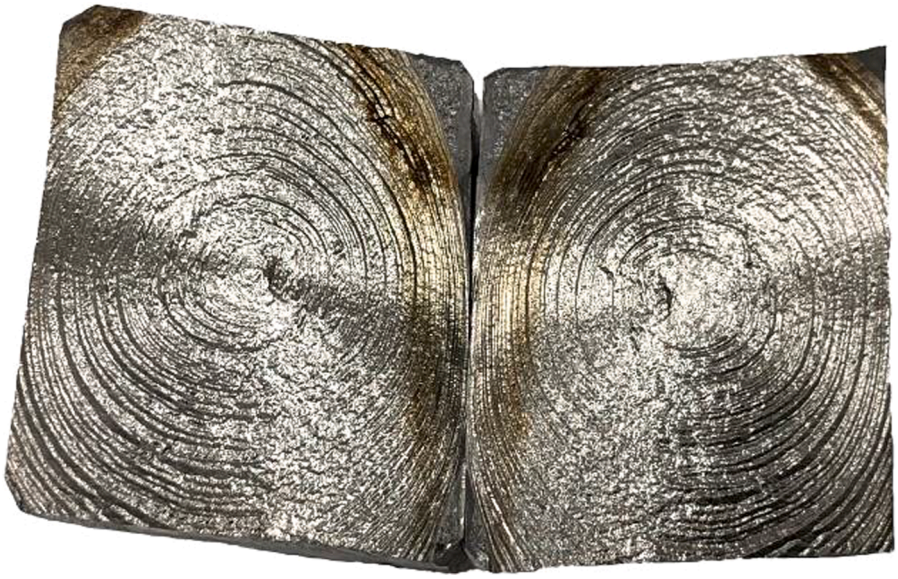

Fig. 3. Morphology of the opening crack surface.

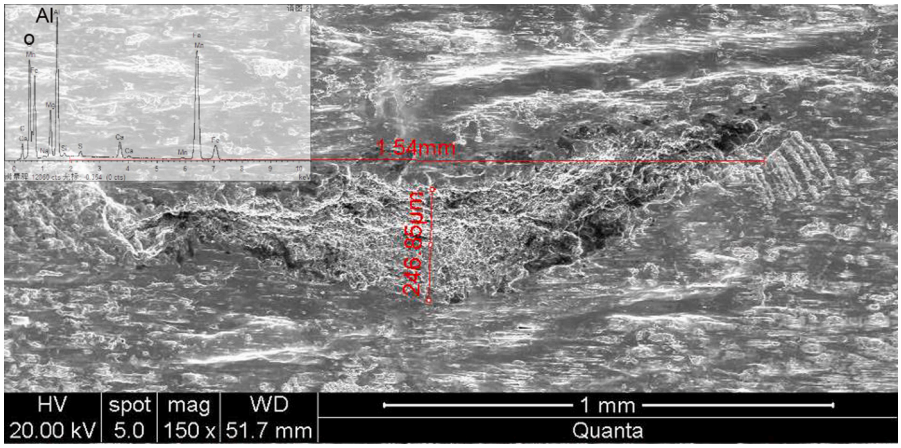

Fig. 4. One defect at initiation zone of shattered rim got by SEM, Insets showing the EDS result of defect.

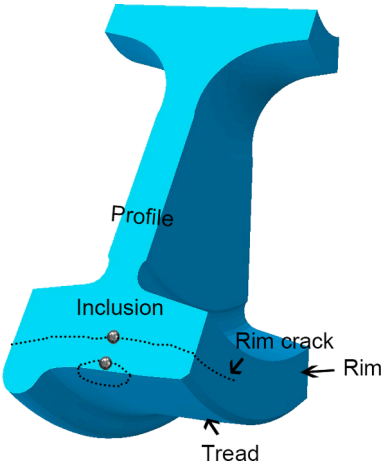

Fig. 5. Schematic of shattered rim and shelling induced by defects.

3. Damage tolerance and remain fatigue life assessment

3.1. Stress simulation of wheel/rail contact

The geometry model of the wheel/rail system containing twenty thousand units with eight nodes was built by software Solidworks. The wheel diameter was 860 mm. Due to the nonlinear factors of the contact analysis, the contact surface of wheel/rail model needed to be refined. The element size of the wheel/rail model in the contact area was 1 mm × 1 mm and its average element size was 5 mm for other areas which were far enough from the stress concentration caused by contact region. Furthermore, for the efficiency of calculation, 1/6 model of the wheels was used for the simulation based on the symmetry of the mode, as shown in Fig. 6. The vertical load was assumed to be the maximum design load, which was 15 ton. A Coulomb friction model was used in ABAQUS, in which the friction stress was proportional to the vertical pressure stress. The hub position was coupled with the hub surface by a node. The axle load with the maximum design value and the rotation speed of the wheel was applied through the coupling point.

The defects which caused shattered rim crack were modeled as pores in this study. Hence, a pore was put in the finite element model for stress analysis. Fig. 7a represented the Von-Mises stress distribution near the pore with a diameter of 2 mm and a distance of 10 mm from the wheel tread. Meanwhile, the curve which showed stress variation along the radial direction below the tread was plotted in Fig. 7b. The results declared that Von-Mises stress decreased gradually with an increasing depth from the tread. It was seen that the stress concentration occurs around the defect. The maximum stress was 650 MPa at the tread and the maximum stress surrounding the defect was 400 MPa. The Von-Mises stress was very small about 50 MPa for the depth of 25 mm from the tread. The multiaxial stress consists of a pressure stress in the radial direction, a shear stress in axle direction and a shear stress in circumference direction. Fig. 7c presents the crack growth rate curve of the wheel steel for the simulation of the crack growth later.

As mentioned above, the fracture surfaces for the case of interior and subsurface crack initiation are different, which is attributed to the stress distribution of rolling contact loading. Here, finite element method was applied to analyze the stress around the contact surface. The results in Fig. 7 indicated that only a small region of the contact location bears high stress, the maximum stress located at the depth of about 2 mm while the stress in the other parts of the wheel is almost zero. Fig. 7b presents the stress variation along the radial direction of the wheel. For the case of shelling (subsurface crack initiation) with the depth 0–10 mm, the pressure stress is very

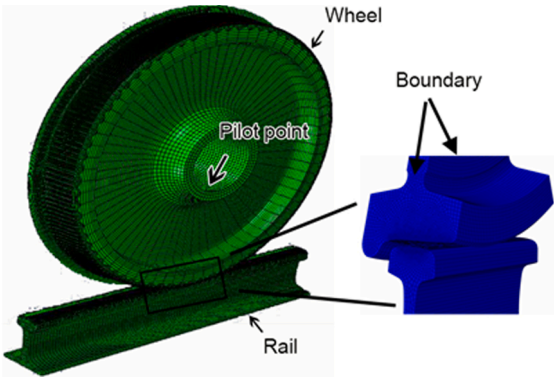

Fig. 6. Finite element modeling of wheel/rail contact system.

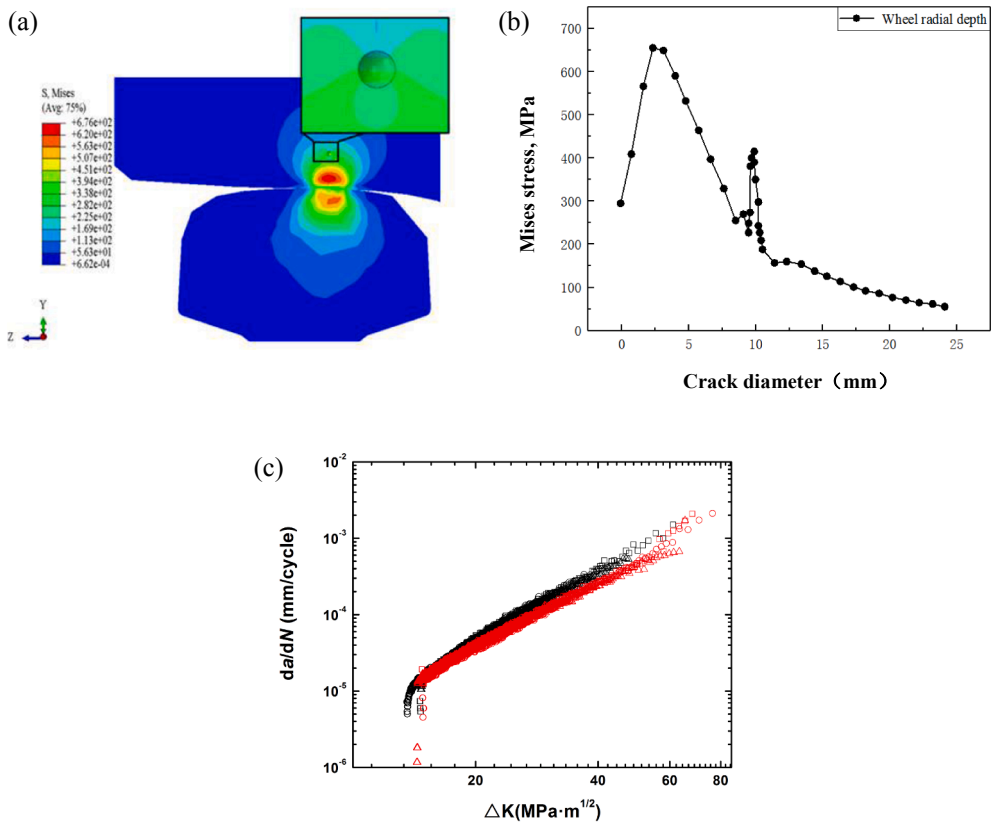

Fig. 7. Von-Mises stress distribution at the defect, (a) front section view, (b) stress variation along the radial direction of the wheel and (c) crack growth rate curve of the wheel steel.

high and decreases with the increase of the depth. The existence of the high pressure will cause the severe plastic deformation near the tread and the press of the crack surfaces. The two shear stress increase first from the tread surface to the 2 mm depth of the wheel, and the maximum shear stress occurs at about 2 mm depth from the tread. These two shear stresses are the driven force of the subsurface crack initiation and propagation.

3.2. Validation of crack propagation simulation

Software FRANC3D was used for the analysis of crack propagation, crack tip SIF and residual fatigue life. According to the method of sub-model, there was no need to remesh of the overall finite element model during the simulation process. It's just necessary to separate a part of overall model and refine the mesh to improve the simulation accuracy. The process of FRANC3D simulation was shown in Fig. 8. The size and location of the initial crack zone was measured by actual data. The model with prefabricated defects processed by FRANC3D was then brought into ABAQUS for further simulation analysis. Subsequently, the crack propagation path, residual fatigue life and crack tip SIF in the model could be obtained through FRANC3D.

The type of crack propagation inside the wheel under rolling contact was a mixed mode, which included three judgment basis: maximum circumferential stress criterion, maximum energy release rate criterion and strain energy density theory. The energy release rate of crack propagation, referred to as G, was the rate at which energy was transformed as a material undergoes fracture, that is, the energy-per-unit-area. As shown in equation (1), in the process of crack propagation, ∂W was the work with external force. On the one hand, this work was used for the change of the elastic strain energy ∂U_e of the system; on the other hand, due to the increased of the crack propagation area, it was used to consume plastic work $r_p \partial A$ and surface energy $r_s \partial A$.

$$\partial W = \partial U_e + (r_p + 2r_s)\partial A \tag{1}$$

According to Irwin's theory of the relationship between the energy release rate G and the stress intensity factor K, Zhao [29] proposed the fracture criterion under the mixed mode loading condition:

$$G(r) = \frac{1-\upsilon^2}{E}\left(\frac{\pi - r}{\pi + r}\right)^{r/\pi} \times \left\{ \left(\frac{2}{3 + cos^2 r}\right)^2 \left[K_1^2(1 + 3cos^2 r) + 4K_1K_2 sin2r + K_2^2(9 - 5cos^2 r)\right] + \frac{1}{1-\upsilon}K_3^2 \right\} = 0 \tag{2}$$

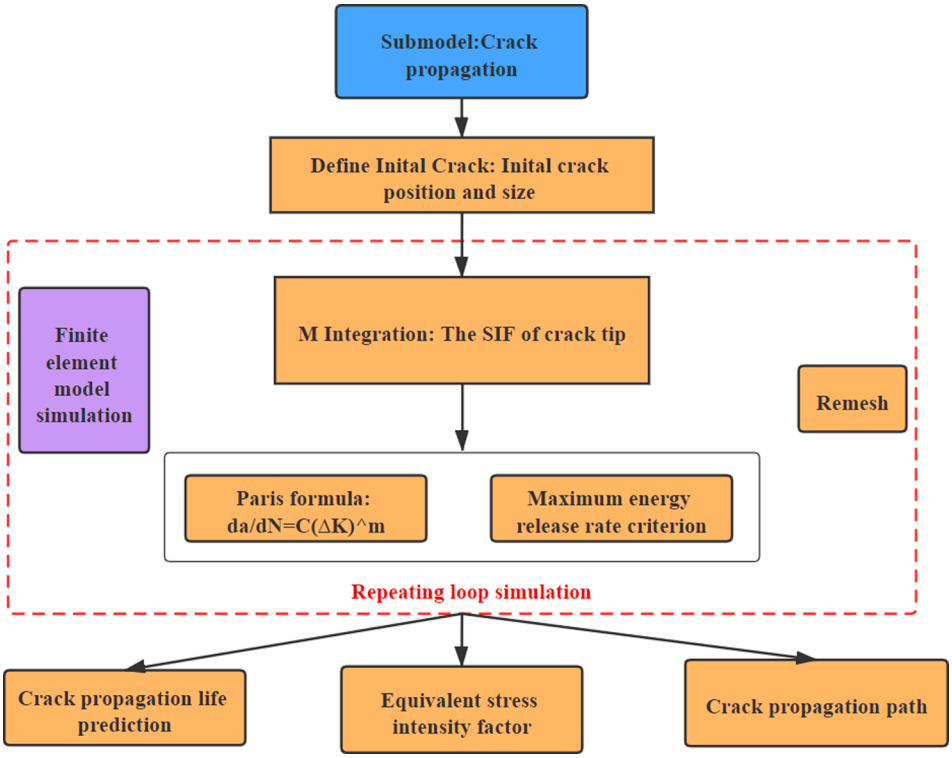

Fig. 8. The simulation process of fatigue crack propagation in wheel rolling contact.

where $\boldsymbol{r}$ was the crack angle, K_I, K_{II}, and K_{III} are the stress intensity factor of Mode I, II and III crack.

The path of crack propagation was along the maximum energy release rate based on the *Griffith-Ivan* theory. The formula of the *MG* criterion (maximum energy release rate criterion) could be derived from the Griffith-Irwin theory and then equation (2) was got.

$$\left(\frac{\pi - r_0}{\pi + r_0}\right)^{r/\pi} \times \left\{ \left(\frac{2}{3 + cos^2 r_0}\right)^2 \left[K_1^2(1 + 3cos^2 r_0) + 4K_1 K_2 sin2r_0 + K_2^2(9 - 5cos^2 r_0)\right] + \frac{1}{1-\upsilon} K_3^2 \right\} = K_{IC}^2 \tag{3}$$

where $\boldsymbol{r_0}$ was the crack angle.

Software FRANC3D had a variety of models for life prediction such as *Forman-Newmande*, *Koning*, *Paris*, *Sinh*, etc. The crack propagation fatigue life of the wheel was predicted by the relationship between the crack size and the number of cycles. In this study, *Paris* formula was used to simulate crack propagation and predict the residual fatigue life of the wheel. Besides, the stress intensity factor amplitude ΔK of the crack tip could be obtained by the stress range $\partial\sigma$ and the crack size a. The stress range $\partial\sigma$ was determined by the stress amplitude of the wheel/rail at the defect.

$$da/dN = C(\Delta K)^m \tag{4}$$

$$\Delta K = K_{max} - K_{min} = Y\sigma_{\max}\sqrt{a} \text{ - } Y\sigma_{min}\sqrt{a} = Y\Delta\sigma\sqrt{a} \tag{5}$$

where C and m were material parameters, which are varied for the different crack propagation stage. Y is the geometric factor and the factor sqrt(π) is included in the geometric factor Y.

There were two thresholds in the crack propagation process. When the crack tip SIF amplitude (ΔK) was less than the fatigue crack propagation threshold ΔK_{th}, the crack would remain the same. However, when ΔK was more than fracture toughness K_{IC}, cracks would propagate rapidly. Consequently, it had two possibilities during the crack propagation process. The crack propagation threshold of steel wheel was 7.7 MPa m $^{1/2}$, and the fracture toughness was 60 MPa m $^{1/2}$. Therefore, it would continue to propagate when ΔK was between ΔK_{th} and K_{IC}. When ΔK was less than ΔK_{th}, the crack stopped growing. When ΔK was greater than ΔK_{th}, the crack quickly propagated and the iteration begins.

As mentioned before, the actual crack source of the wheel rim crack was 16.7 mm depth from the tread and 60.3 mm from the outer side of the rim. The size of the inclusions was 1.54 mm long and 0.25 mm wide. The service mileage of this wheelset was 550,000 km. The location and size of inclusion in the case of shattered rim was chosen as initial conditions for numerical simulation of crack propagation, and the initial crack was equivalent to an ellipse with the same area as the actual inclusion [22,23], as shown in Fig. 9a. It was demonstrated that the crack propagation path in the simulation was corresponded to that in the actual shattered rim case. As for

the distance in the simulation, the results showed that the number of loading cycles was 2.56×10^8 (about 670,000 km in service). It was obviously close to the actual value. From Fig. 9b, the wheel life under different crack lengths was computed and plotted. It showed that the crack propagation rate was slow in the early stage and became rapid when the crack length reached a certain value in the later stage. The crack critical size of shattered rim and detection cycle can be confirmed via the curve. When the initial crack diameter 2a (the crack size and length in this article refer to its diameter) reached to 2.0 mm, the crack propagation rate increases significantly. Consequently, the fatigue life of the wheel obtained by the simulation was small, which accords with the discipline of fatigue crack propagation. The simulation method can be used to predict the fatigue life of a wheel and study the influence of the parameters (the initial crack position and crack size) on the fatigue life.

3.3. Influence of the initial size and position of the crack on wheel fatigue life

In order to consider the influence of different initial crack sizes on the fatigue life of the wheel, circular cracks with initial lengths of 2a = 0.2 mm, 0.6 mm, 2.0 mm were respectively set at a position of 20 mm from the wheel tread to simulate the crack propagation life. The simulation result was shown in Fig. 10a. The initial stage of crack propagation was very steady and consumed most of the fatigue life. Meanwhile, the crack length basically did not change. As the crack reached to a considerable value, the crack propagation rate increased rapidly, and the residual life of the wheel was only a small fraction of its total fatigue life. As shown in Fig. 10b, the stress intensity factor (SIF) amplitude increased with the growth of the crack diameter, which is consistent with the trend of fatigue crack propagation. It was appeared that the main reason for the increase of crack propagation rate was the increase of the stress intensity factor.

Fig. 9a shows that the fatigue life of wheels with an initial crack diameter of 0.2 mm and 2.0 mm was significantly different. When the initial defect size 2a are 0.2, 0.6 and 2.0 mm, the corresponding cycle number $\boldsymbol{N}$ are 1.6×10^9, 3.0×10^8, 8.0×10^7, respectively. From the above simulation results, it was seen that for ultra-high cycle fatigue, the initial stage of fatigue crack propagation accounted for a large proportion of the total fatigue life. In addition, the size of the initial crack had a great impact on the fatigue life, and the smaller the initial crack size, the longer the fatigue life was.

When the initial defects were at different depths from the tread, the fatigue life of the wheel varies greatly. A circular crack with an initial diameter of 1 mm was set at the depths of $d_0 = 5.0$, 10.0 and 20.0 mm from the wheel tread to simulate its fatigue crack propagation life. The simulation results were shown in Fig. 11. Comparing Fig. 10a and b, it could be concluded that as the depth of the initial defect from the tread increased, the fatigue life of the wheel increased at the same time. However, the SIF value decreased with the increase of the depth of the crack from the tread surface, when the crack diameter was less than 6 mm. When the crack diameter was greater than 6 mm, the SIF value of the crack at the depths of 10 and 20 mm from the tread was greater than the SIF value of the crack at the depth of 5.0 mm from the tread. In addition, when the depths of the crack from the tread was 5.0, 10.0, 20.0 mm, the cycles of the loading were above 1.2×10^8, 1.7×10^8, 2.2×10^8, respectively.

Consequently, the location of the initial crack had a significant impact on the life of the wheel with the rim crack. When the initial crack was close to the wheel tread, its fatigue life was reduced. It could be seen from the finite element simulation that the stress increased when the initial crack located near to the wheel tread, and the magnitude of the stress intensity factor also increased.

3.4. The assessment of wheel damage tolerance and remaining fatigue life

The initiation of cracks caused by inclusions and pores of different sizes generally located at a depth of 15–20 mm from the tread [15,17]. A crack with an initial length of 0.6 mm at a position of 20 mm from the wheel tread was set as a case, and its crack propagation curve was shown in Fig. 12a. The curve in Fig. 12 had an obvious turning point, which meant that there were two stages in the crack propagation process: steady propagation stage and rapid propagation stage. The number of cycles was 2.6×10^8, corresponding to a wheel work mileage of 710,000 km, when the crack diameter propagated from 0.6 mm to 2.0 mm. However, when the

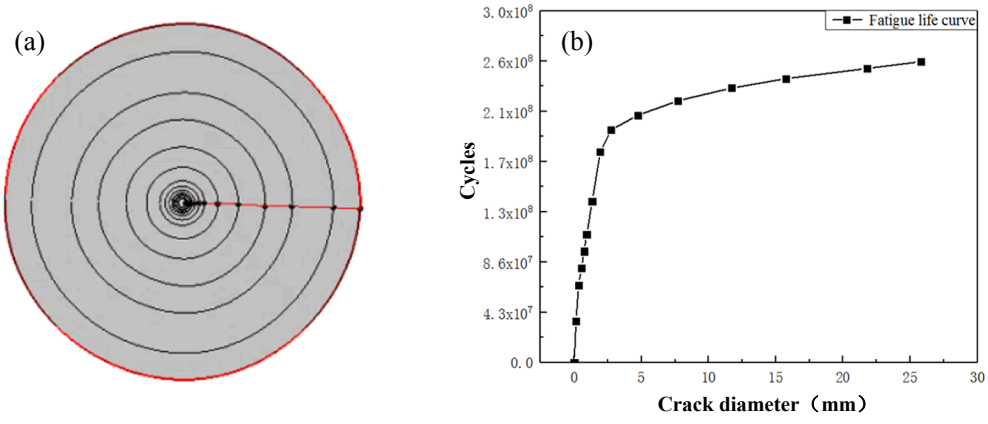

Fig. 9. Fatigue crack propagation life prediction: (a) crack propagation path, (b) relationship between crack length and wheel life.

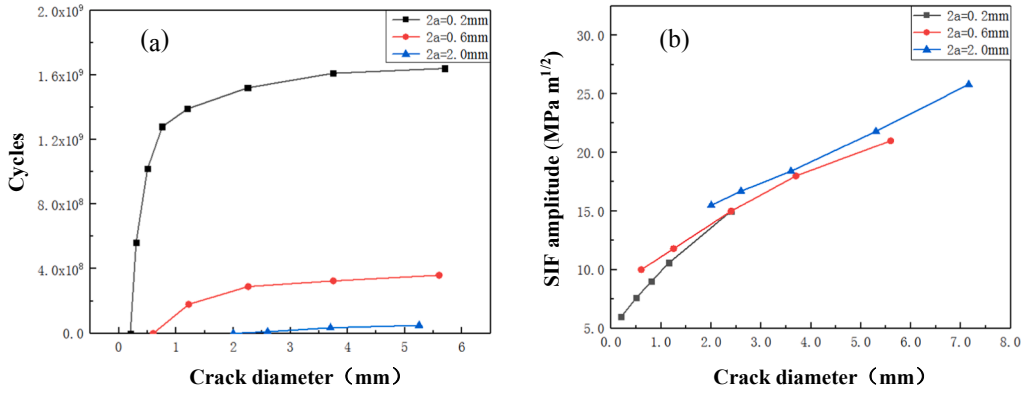

Fig. 10. Fatigue life of a wheel with different initial crack diameters: (a) relationship between cycles of the loading and crack diameters, (b) relationship between equivalent SIF and crack diameters.

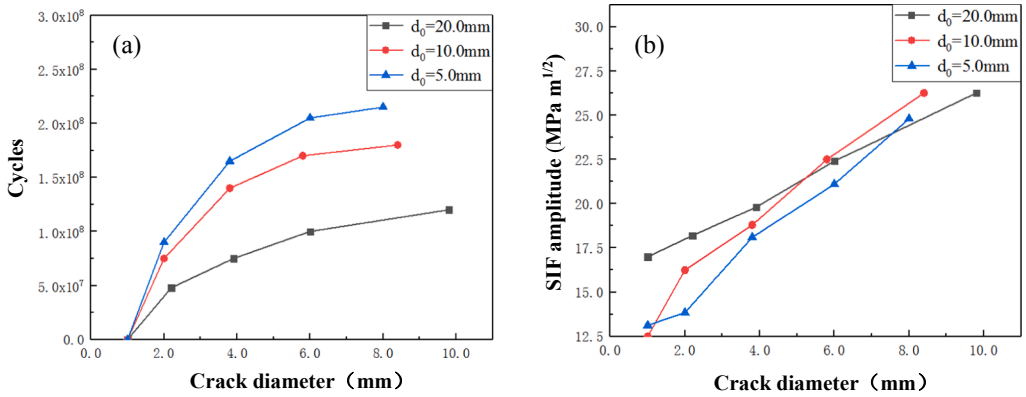

Fig. 11. Fatigue life of a wheel under different initial depths of the crack from the tread:(a) relationship between cycles of the loading and different depths of the crack from the tread, (b) relationship between the equivalent SIF and different depths of the crack from the tread.

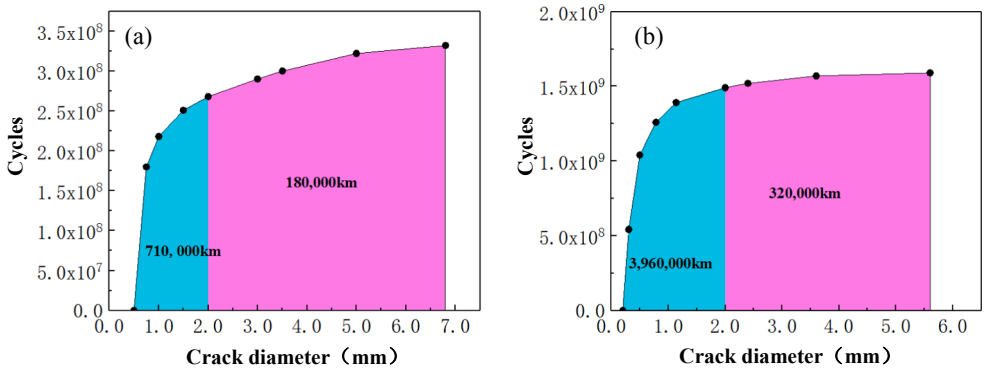

Fig. 12. Crack propagation curve for the crack at the depth of 20 mm from the tread:(a) the initial diameter of the crack is 0.6 mm, (b) the initial diameter of the crack is 0.2 mm.

crack diameter propagated from 2.0 mm to 6.8 mm, the number of cycles was 7×10^7, which was equivalent to a wheel work mileage of 180,000 km. Therefore, in the initial stage, the crack propagation rate was slow, the diameter of the crack was relatively small, and this stage occupied most of the total life of the wheel. In the following process, the crack propagation rate gradually increasing, the remaining stage accounted only for a small part of the service life of the wheel. Thus, the threshold of crack propagation from the former stage to the later stage was defined as the damage tolerance.

When the diameter of the internal crack was less than 2 mm, the wheel served safely, and its residual fatigue life was worthy of

attention. The residual fatigue life of the wheel could be got from the crack propagation curve. According to Fig. 11a, the cyclic of the loading was 5×10^7, which was corresponding to a wheel work mileage of 135,000 km. In other words, if the crack inside the wheel is detected by the inspection equipment, the wheel can only run 135,000 km corresponding to the propagation from 1.0 mm to 2.0 mm. It should be paid attention that not only the position and size of the initial crack, but also the actual service load and wheel/rail conditions that affected the damage tolerance and residual life of the wheel.

In the article, this method could be used to evaluate the specific inclusions inside the wheel, and whether the wheel was safe or not during service. As shown in Fig. 12b, a crack with a diameter of 0.2 mm was set at the depth of 20 mm from the wheel tread. When the crack diameter changed from 0.2 mm to 2 mm, the number of cyclic loads was 1.47×10^9, which was equivalent to a wheel work mileage of 3.96 million kilometers. However, the current full-life service distance of wheel was about 2 million kilometers. It could be seen that the wheels operated safely throughout the service cycle.

4. Conclusion

Based on the failure analysis of the wheel rim crack of the Chinese train, the software ABAQUS was used to analyze the wheel-rail contact stress distribution with inclusion defects in the wheel, and the software FRANC3D was used to simulate the fatigue crack propagation. Researches on the evaluation of the damage tolerance and remain fatigue life of the railway wheel under rolling contact loads was conducted. The conclusions are as follows:

(1) The failure analysis of rims showed that the cracks originated from alumina inclusions inside the rims, the size of which was above the value in standard. fatigue life corresponding to the service mileage was over 10^7.
(2) The distribution of contact stress increased at first and then decreased as the depth of the defects from the tread surface increased, and the stress concentration near the inclusion was obvious.
(3) With the increase of the initial crack size, the fatigue life of the wheel decreased significantly. The fatigue life reached more than 10^9 cycles when the initial crack length was 0.2 mm, and the fatigue life was about 10^7 cycles when the initial crack length was 2.0 mm. With the increase of initial crack depths, the fatigue crack life also increased obviously. The fatigue cycles were more than 1.2×10^8, 1.7×10^8 and 2.2×10^8 when the initial crack depth was 5, 10 and 20 mm from the tread surface, respectively.
(4) Based on the crack propagation curves obtained by simulation, a method for analysis of the fatigue damage tolerance of the wheel and the remaining life evaluation was developed. The critical dimension of the initial crack propagation into the rapid expansion of 2 mm was taken as the damage tolerance of the wheel rim crack when the crack is in the depth of 10 mm.

Declaration of Competing Interest

The authors declare that they have no known competing financial interests or personal relationships that could have appeared to influence the work reported in this paper.

Acknowledgments

The authors would like to acknowledge financial support from the Development Project of China Railway (No. J2019J004) and the China Academy of Railway Sciences Corporation Limited (No. 2019YJ097), the National Natural Science Foundation of China (No. 11802011).

References

[1] L. Ma, C.G. He, X.J. Zhao, J. Guo, Y. Zhu, W.J. Wang, Q.Y. Liu, X.S. Jin, Study on wear and rolling contact fatigue behaviors of wheel/rail materials under different slip ratio conditions, Wear 366–367 (2016) 13–26.
[2] B. Zhang, X.Q. Fu, Type and formation mechanism of railway wheel and tire tread spall, China Railway Sci. 02 (2001) 76–81.
[3] W.J. Wang, Q.Y. Liu, Research review on wheel tread spalling, Machinery 31 (6) (2004) 12–15.
[4] T. Makino, M. Yamamoto, T. Fujimura, Effect of material on spalling properties of railroad wheels, Wear 253 (1) (2002) 284–290.
[5] E. Lansler, E. Kabo, Subsurface crack face displacements in railway wheels, Wear 258 (7) (2005) 1038–1047.
[6] Y.G. Wang, C. Lu, X. Zhao, Rolling congtact fatigue of chinese high speed wheels: observations and simulations, J. Mech. Eng. 45 (4) (2018) 150–157.
[7] D. Stone, C. Lonsdale, S. Kalay, Effect of wheel impact loading on shattered rims, in: Proceedings of the 13th International Wheelset Congress, 2001, pp. 17–21.
[8] S.P. Zhu, S. Foletti, S. Beretta, Evaluation of size effect on strain-controlled fatigue behavior of a quench and tempered rotor steel: Experimental and numerical study, Mater. Sci. Eng., A 735 (2018) 423–435.
[9] L. Patriarca, M. Filippini, S. Beretta, Short-crack thresholds and propagation in an AISI 4340 steel under the effect of SP residual stresses, Fatigue Fract. Eng. Mater. Struct. 41 (6) (2018) 1275–1290.
[10] S.C. Wu, Z.W. Xu, C. Yu, O.L. Kafka, W.K. Liu, A physically short fatigue crack growth approach based on low cycle fatigue properties, Int. J. Fatigue 103 (2017) 185–195.
[11] S.C. Wu, Z.W. Xu, Y.X. Liu, G.Z. Kang, Z.X. Zhang, On the residual life assessment of high-speed railway axles due to induction hardening, Int. J. Rail Transp. 6 (4) (2018) 218–232.
[12] S. Beretta, Application of multiaxial fatigue criteria to materials containing defects, Fatigue Fract. Eng. Mater. Struct. 26 (6) (2010) 551–559.
[13] A. Ekberg, E. Kabo, J.C.O. Nielsen, R. Lundén, Subsurface initiated rolling contact fatigue of railway wheels as generated by rail corrugation, Int. J. Solids Struct 44 (24) (2007) 7975–7987.
[14] J.C.O. Nielsen, A. Ekberg, R. Lundén, Influence of short-pitch wheel/rail corrugation on rolling contact fatigue of railway wheels, Proc. Inst. Mech. Eng. Part F-J. Rail Rapid Transit. 219 (3) (2005) 77–187.
[15] E. Kabo, A. Ekberg, Material defects in rolling contact fatigue of railway wheels—the influence of defect size, Wear 258 (7) (2005) 1194–1200.

[16] A. Ekberg, E. Kabo, H. Andersson, An engineering model for prediction of rolling contact fatigue of railway wheels, Fatigue Fract. Eng. Mater.. Struct. 25 (10) (2010) 899–909.
[17] T. Cong, J.M. Han, Y.S. Hong, J.P. Domblesky, Shattered rim and shelling of high-speed railway wheels in the very-high-cycle fatigue regime under rolling contact loading, Eng. Fail. Anal. 97 (2019) 556–567.
[18] T. Cong, J.M. Han, G. Chen, Study on performance of new material wheel for high speed electric multiple unit, China Railway Sci. 39 (1) (2018) 75–81.
[19] T. Cong, J.M. Han, G.Z. Zhang, Analysis of micro damage factors of shattered rim and tread shelling of railway whee, China Railway ence 38 (5) (2017) 93–99.
[20] T. Makino, Y. Neishi, D. Shiozawa, S. Kikuchi, H. Saito, K. Kajiwara, Y. Nakai, Rolling contact fatigue damage from artificial defects and sulphide inclusions in high strength steel, Procedia Struct. Integr. 7 (2017) 468–475.
[21] I. Bodini, A. Mazzù, C. Petrogalli, M. Lancini, T. Kato, T. Makino, A study of wear and rolling contact fatigue on a wheel steel in alternated dry-wet contact aided by innovative measurement systems, Procedia Struct. Integr. 18 (2019) 849–857.
[22] Y. Murakami, N.N. Yokoyama, J. Nagata, Mechanism of fatigue failure in ultralong life regime, Fatigue Fract. Eng. Mater. Struct. 25 (8–9) (2002) 735–746.
[23] Y.M. Liu, L.M. Liu, S. Mahadevan, Analysis of subsurface crack propagation under rolling contact loading in railroad wheels using FEM, Eng. Fract. Mech. 74 (17) (2007) 2659–2674.
[24] Y.M. Liu, L.M. Liu, B. Stratman, S. Mahadevan, Multiaxial fatigue reliability analysis of railroad wheels, Reliab. Eng. Syst. Saf. 93 (3) (2008) 456–467.
[25] S.X. Zhou, Equivalent stress evaluation of the load spectrum measured on the EMU axle based on damage tolerance, J. Mech. Eng. 51 (8) (2015) 131.
[26] D.K. Liu, Life prediction method for EMU axle box bearings based on actual measured loadings, J. Mech. Eng. 52 (22) (2016) 45.
[27] H.L. Sun, M. Tang, The adavantage of new development for china high-speed railway, Study Times (2018).
[28] H.W. Zhao, J.Y. Liang, C.Q. Liu, High-speed EMUs: characteristics of technological development and trends, Engineering 6 (3) (2020) 234–244.
[29] Y.S. Zhao, The application of maximum energy release rate criteria in the fracture caused by mixed mode II-III and I-II-III cracks, Mech. Eng. 3 (1985) 20–22.